Fabrication of surfactant-polyelectrolyte complex using valvejet 3D printing-aided colloidal self assembly

Vadodaria, Saumil Sudhir; He, Yinfeng; Mills, Tom; Wildman, Ricky

DOI:
10.1016/j.colsurfa.2020.124914

Document Version
Peer reviewed version

Citation for published version (Harvard):
Vadodaria, SS, He, Y, Mills, T & Wildman, R 2020, 'Fabrication of surfactant-polyelectrolyte complex using valvejet 3D printing-aided colloidal self assembly', *Colloids and Surfaces A: Physicochemical and Engineering Aspects*, vol. 600, 124914. https://doi.org/10.1016/j.colsurfa.2020.124914

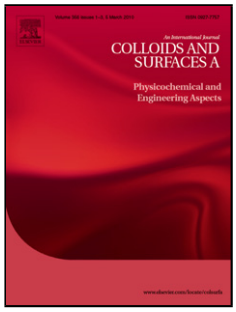

Fabrication of Surfactant-Polyelectrolyte Complex using Valvejet 3D Printing-Aided Colloidal Self Assembly

Saumil Sudhir Vadodaria (Conceptualization) (Investigation) (Writing - original draft), Yinfeng He (Methodology) (Resources)<ce:contributor-role>Writing - review and editing), Tom Mills (Supervision)<ce:contributor-role>Writing - review and editing) (Funding acquisition), Ricky Wildman (Supervision)<ce:contributor-role>Writing - review and editing) (Funding acquisition)

PII: S0927-7757(20)30507-0

DOI: https://doi.org/10.1016/j.colsurfa.2020.124914

Reference: COLSUA 124914

To appear in: *Colloids and Surfaces A: Physicochemical and Engineering Aspects*

Received Date: 21 March 2020

Revised Date: 22 April 2020

Accepted Date: 24 April 2020

Please cite this article as: Vadodaria SS, He Y, Mills T, Wildman R, Fabrication of Surfactant-Polyelectrolyte Complex using Valvejet 3D Printing-Aided Colloidal Self Assembly, *Colloids and Surfaces A: Physicochemical and Engineering Aspects* (2020), doi: https://doi.org/10.1016/j.colsurfa.2020.124914

Fabrication of Surfactant-Polyelectrolyte Complex using Valvejet 3D Printing-Aided Colloidal Self Assembly

Saumil Sudhir Vadodaria *[a], *Yinfeng He* [b], *Tom Mills* [a] *and Ricky Wildman* [b]

[a]School of Chemical Engineering, University of Birmingham, Birmingham, United Kingdom B15 2TT

[b]Department of Mechanical, Materials and Manufacturing, University of Nottingham, Nottingham, United Kingdom NG8 1BB

s.vadodaria@bham.ac.uk, yinfeng.he@nottingham.ac.uk, t.b.mills@bham.ac.uk, ricky.wildman@nottingham.ac.uk.

Phone number of the corresponding author: 0044 7966 478 376.

Graphical abstract

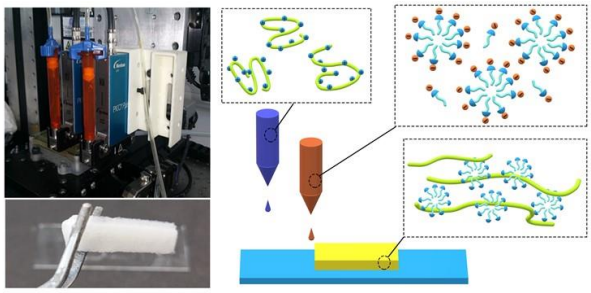

Abstract

Complexes consisting oppositely charged surfactants and polyelectrolytes (SPEC) have potential as delivery vehicles for drugs, nutrients and flavours. However, conventional methods for their fabrication often introduce microstructural irregularities owing to poor diffusion of components. Thus, controlled-release capabilities of SPEC cannot be fully realised.

Valvejet 3D printing enables spatially and quantitatively controlled layer-by-layer deposition of fluid droplets. Using this technique, alternating layers of chitosan and sodium dodecyl sulphate solutions were 3D printed over one another. Printed specimens were characterised along with control specimens (prepared by film casting) using confocal microscopy, cryo-SEM and elemental analysis.

3D printed samples were found to contain a previously unreported network of interconnected SPEC microcapsules forming a mechanically strong specimen. Micro-CT images confirmed that microcapsules with similar diameter spanned the entire specimen. Control sample was found to

have no such microstructure. Elemental analysis revealed that printed sample had excess polyelectrolyte whereas control sample had excess surfactant.

Keywords

3D Printing, Additive Manufacturing, Valvejet, Pneumatic Jet, Surfactant-Polyelectrolyte Complexes, Self-Assembly, Confocal Microscopy, Cryo-SEM, Micro-CT.

Introduction

Complexes formed by mixing charged surfactants with oppositely charged polyelectrolytes are particularly exciting supramolecular assemblies as they incorporate both electrostatic and hydrophobic interactions. The surfactant-polyelectrolyte complexes (SPEC) have been widely used as rheology modifiers and vehicles for active agents, rendering them relevant to pharmaceutical, personal care and nutritional applications [1].

At low concentrations, the formed SPEC are soluble. However, they tend to precipitate beyond what is termed as the critical aggregation concentration (CAC) [2]. Such CAC lies below the critical micelle concentration, i.e. CMC of surfactants. At even higher concentration, mixing the solutions of polyelectrolytes and surfactants can lead to formation of SPEC film/microcapsules at the solution interface [3–5].

Of the most common conventional methods for SPEC fabrication is drop-wise addition/spraying of either polyelectrolyte or surfactant solution into the other [2,4–8]. The purpose of such a preparation is often to produce mini- and microcapsules of SPEC as they derive their shape from

that of the droplet. There are also many reports of macroscopic mixing (i.e. mixing large quantities of solutions of both components followed by mechanical stirring) technique [9–12].

When solutions of surfactant and polyelectrolyte come into contact, SPEC formation initiates but does not necessarily complete instantaneously as the polyelectrolyte solution is often too viscous to allow instantaneous diffusion of both species. Moreover, the formation of SPEC film at the interface progressively slows down the diffusion as the film thickness keeps growing [5,6]. The colloidal self-assembly relies heavily on the degree of diffusion. Poor diffusion often causes formation of localised regions of unreacted polyelectrolyte/surfactant in SPEC. Excess of either of these, especially of surfactant in contact with the SPEC surface may result in SPEC disintegration by redissolution [3]. Similarly, the supernatant released following the complex formation may get trapped inside the 'pockets' of SPEC films owing to poor permeability. Overall, the structure of SPEC formed using conventional methods is often abundant with microstructural irregularities. This makes it difficult to realise the full potential of SPEC in applications where structural homogeneity is essential.

Thus, mixing the solutions containing both charged components in as small a quantity as possible (thereby maximising their interfacial area in contact) could render their diffusion more complete and much faster by reducing diffusion distance, thereby aiding the colloidal self-assembly. This is likely to improve the structural regularity of SPEC. The most widely used technique for this till now is layer-by-layer (LbL) dip coating of polyelectrolyte and surfactant on a flat surface [7,13–16]. This technique involves dipping of a flat substrate in solutions/suspensions of the substance to be deposited followed by rinsing and/or drying. This needs to be done sequentially and repeatedly according to the desired arrangement for the layers. Hence, fabrication of a film thicker than 1 mm using this method is prohibitively time consuming for practical purposes [17].

Therefore, the application of LbL technique for SPEC preparation has been largely limited to developing hydrophobic coatings and films [18] rather than creating macroscopic shapes. Films have also been prepared by casting non-aqueous solutions of SPEC on various surfaces followed by drying [19] but this method needs much time to allow solvent evaporation.

It is therefore vital to employ a manufacturing technique for SPEC which still deposits the materials layer-by layer but with much higher throughput and is commercially viable. Deposition by controlled jetting of the solution components (i.e. printing) is a technique of choice for such requirement.

Conventional inkjet systems typically require the shear viscosity of ink to be below 0.04 Pa.s. Semi-dilute to concentrated solutions of the vast majority of moderate-to-high molecular weight polyelectrolytes are expected to have much higher viscosity, being unsuitable for inkjet printing. This could well be the reason why SPEC in entirety have not been reported yet to be prepared using inkjet printing. In the process closest to 3D printing which was utilised for SPEC in the past [14], a layer of polyelectrolyte was prepared by electrodeposition and a surfactant solution was printed over it using microextrusion. While they were able to generate SPEC, the electrodeposition step considerably slowed the process.

Valvejet printing is a deposition system analogous to conventional inkjet printing but is capable of handling fluids with much higher viscosity (0.05 – 500 Pa.s) [20]. The greater ejecting force of valvejet originates from adjustable pneumatic pressure applied on to the fluid as opposed to conventional inkjet with no pneumatic force. The droplet generation and break-up are governed by an orifice-valve mechanism with a piezoelectric actuator. Use of voltage wave-forms helps achieve high jetting frequency [20]. Such valve-dispensing technique has already been used in the

past for printing drug nanosuspensions [21], silicone-based fluids [22] and a photo-reactive resin based conductive material [23]. These fluids have a wide range of rheological properties and microstructures, showing the versatility of this technique.

There is an increasing awareness about the potential of additive manufacturing in late-stage customisation of medicine at a pharmacy or hospital. Such customisation is helpful for fulfilling individual therapeutic needs [24,25] and is commercially advantageous [26]. SPEC applications as the delivery vehicle for active compounds have the potential to be exploited further by use of additive manufacturing. The present study explores valvejet-based 3D printing as a technique for layer-by-layer fabrication of SPEC. This work will aim at printing specimens with height of a few mm and their characterisation.

Sodium dodecyl sulphate (SDS), a widely reported anionic surfactant will be used in the present study. Chitosan will be used as the corresponding cationic polyelectrolyte. Chitosan is a polysaccharide derived from partial deacetylation of chitin, a poly (N-acetyl-D-glucosamine). Chitosan has one -NH_2 group per deacetylated repeating unit. While insoluble at neutral pH, -NH_2 groups get protonated under acidic pH and render chitosan water soluble [2]. It has been used in biomedical applications due to its non-toxic and biodegradable nature, as well as its antimicrobial properties and lipase activity [27].

Fungal chitosan is considered to have many advantages over the non-fungal chitosan. Fungal chitosan is free from shrimp protein (an allergen). A greater control over molecular weight and degree of deacetylation of fungal chitosan can be achieved. Also, suitability of biowaste as a raw material makes its production environmentally more sustainable [28]. The present study therefore uses fungal chitosan as one of the reagents for SPEC formation.

SPEC made using chitosan and SDS have already been reported in the scientific literature [2,5,8,12–14,27,29]. However, SPEC using these or other components have never been reported to have been made using techniques analogous to inkjet or valvejet, to the best of the authors' knowledge.

Microstructure of the printed SPEC specimen will be examined by cryogenic scanning electron microscopy and confocal microscopy along with their equivalent samples prepared using film casting as controls. The printed specimen will also be tested using micro computed tomography (Micro-CT) and elemental analysis (CHNS).

Materials and Methods

Materials

Fungal chitosan was obtained from Glentham Life Sciences, UK with ≥ 98.0% of degree of deacetylation and 100-300 cP viscosity at 1% concentration in 1% acetic acid at 20°C according to the supplier. Sodium dodecyl sulphate, acetic acid and Nile Red were bought from Fischer Scientific, UK. Xanthan gum was supplied by Sigma-Aldrich, UK. All these chemicals were used as received without any purification or modification.

Preparation of Inks

A stoichiometric balance of positive charge in chitosan and negative charge in SDS was accounted for while preparing the inks with the aim of producing a charge neutral SPEC. Considering the

volatile content of chitosan (~7.0%) and SDS (~2.5%) as well as degree of acetylation of chitosan, 2.5% (w/w) chitosan solution in 1% (w/w) acetic acid and 4.0% (w/w) of SDS solution were calculated to contain equivalent concentrations of ~0.14 $M.L^{-1}$ active cationic and anionic charges respectively. This calculation was based on the average molecular weight of one repeating unit of chitosan (considering the degree of deacetylation) and the molecular weight of SDS. The volatile content in both cases refers to water and other impurities which can be removed by heating. These impurities were measured gravimetrically and their content was used when preparing the solutions.

Since SPEC being formed are precipitates leaving behind significant amount of supernatant (presumably with trace amounts of chitosan, SDS, xanthan and some acetic acid), increasing the concentration of polyelectrolyte or surfactant leads to less supernatant following complexation. In order to achieve this, the concentration of SDS solution to be prepared was doubled to 8.0% (w/w). However, doubling the concentration of chitosan solution to 5.0% (w/w) was likely to not only make it almost too viscous to print but also likely to delay the surfactant diffusion. The concentration of chitosan was therefore kept at 2.5% (w/w). The revised concentration of SDS solution altered the stoichiometric balance from 1:1 to 2:1 for 2.5% (w/w) chitosan solution:8.0% (w/w) SDS solution.

Ink A was prepared by mixing the required quantity of chitosan with 1% (w/w) aqueous solution of acetic acid. For ink B, stock solutions of (i) 16% (w/w) SDS and (ii) 0.2% (w/w) xanthan gum were prepared separately. They were then mixed in 1:1 proportion by weight to prepare ink B with the final concentration of 8% and 0.1% (w/w) for SDS and xanthan gum respectively. Xanthan gum was intended to act as a viscosifier in ink B in order to improve spatter resistance during printing. Even though xanthan gum itself is an anionic polymer, the charge density on it is very low and hence was considered not to significantly change the stoichiometric balance of the inks at

a mere 0.1% (w/w) concentration. 0.001 M of sodium azide was added in both the inks for microbial resistance. All mixing was performed by magnetic stirrers. The dissolution of chitosan, SDS and xanthan gum was performed overnight and the mixing of two stock solutions into ink B was performed over 3 hours. All subsequent printing was performed using the above formulation of inks.

Ink B to be used for producing confocal microscopy samples had 10 mg of Nile Red stock solution (1 mg/ml Nile Red in acetone) added per 10 ml of the SDS stock solution prior to mixing with xanthan gum solution. Adding fluorescent dyes such as Nile Red is a requirement for confocal microscopy. Nile Red is expected to be embedded within the exterior regions of SDS micelles acting as a probe [30].

Characterisation of Inks

The inks were characterised for their viscosity as well as pH in order to make sure they are suitable for the valve-jet printer and that their mixture would lead to stable SPEC. The viscosities of both inks were measured using Kinexus Pro+ rheometer (Malvern Instruments, UK) through a shear rate sweep at 20°C. Shear rate was logarithmically varied from 0.01 s^{-1} to 1000 s^{-1} with 5 data points per decade of shear rate. The geometry used was DIN concentric cylinders with 25 mm and 27 mm of inner and outer diameters respectively and 40 mm of bob length.

The pH values of both inks were measured using a pH meter (SevenCompact, Mettler Toledo, United Kingdom). Following this, the inks were mixed well in stoichiometric amounts and the pH of the supernatant in mixture was also measured.

Film Casting

10 ml of ink A was poured in a petri dish and was allowed to rest for 60 minutes to form a flat surface. Over this, 5 ml of ink B was laid in a slow, drop-wise manner. The petri dish was kept at the ambient temperature for 48 hours. Following this, the supernatant was removed to expose the film formed at the interface of both the inks.

Two types of cast films were prepared: (i) with ink B containing no fluorescent dye for cryo-SEM and elemental analysis and (ii) with ink B containing Nile Red for confocal microscopy.

The film was cut using a blade to obtain the 'control' samples for characterisation techniques.

Valvejet Printing

The deposition system used was PicoPulse (Nordson, UK) mounted on a three axis motion stage. Each of the two printheads was loaded with syringe containing ink A or B respectively (See Figure 1).

Figure 1. Valvejet printheads with syringes and compressed air supply.

The diameter of the valve orifice was 150 μm for both printheads. Air pressures and other wave form parameters are given in Table 1 in Supporting Information. A detailed explanation of these parameters have been given by Wildman et al. (2013) [20].

A schematics of SPEC formation through printing have been shown in Figure 2. The droplet spacing was set to 450 μm. This was found to be the maximum distance which allows sufficient overlapping between droplets to form a continuous film layer. A rectangular array of 68 x 14 droplets was printed for each layer. Layers of inks A and B respectively were printed in an

alternating fashion. First layer printed was of ink A in order to make it adhere better to the glass surface which is claimed to have mild negative charge.

It was important to deposit the inks in their stoichiometrically balanced amounts, i.e. in 2:1 proportion of ink A:ink B. The amount of ink A printed was measured gravimetrically following 2, 5 and 10 layers of ink A being printed. The average mass of ink A per layer was found to be 0.062 g. This implied the desired amount of ink B deposited to be 0.031 g/layer. To achieve this, the gravimetric measurement was repeated for ink B after after printing 2, 5, and 10 layers. Compressed air pressure for ink B was varied (i.e. increasing pressure for more ink to be deposited and vice versa) in response to the deposited amount per layer being greater or smaller than 0.031 g. 55.2 kPa of compressed air pressure for ink B appeared to achieve 0.031 g of its deposition per layer.

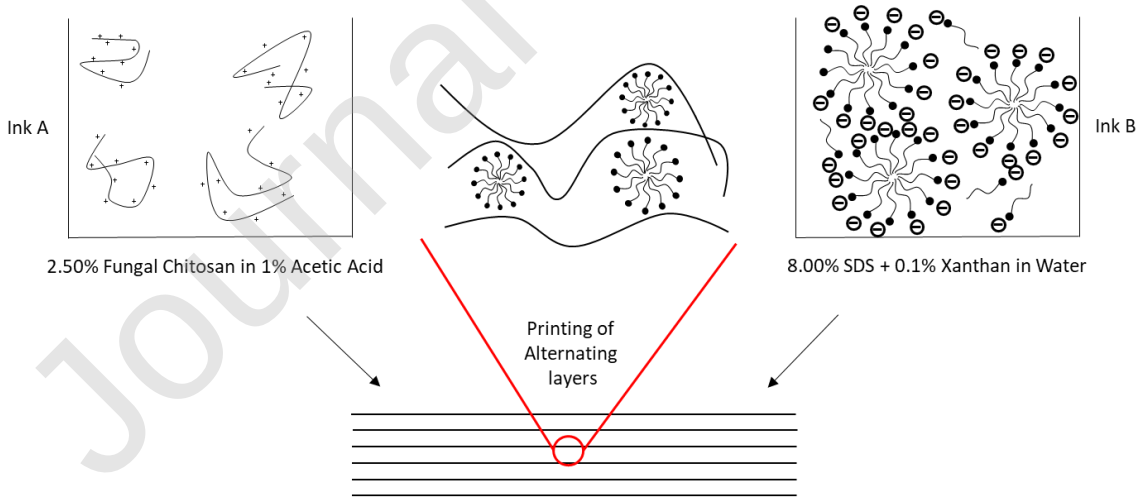

Figure 2. Schematic diagram of printing SPEC using valve-jet printing.

Different shapes of samples were printed to suit different characterisation techniques. For techniques such as CHNS analysis and micro-CT, a specimen was printed with 8 complex layers of abovementioned rectangular array wherein one complex layer constituted one layer for ink A + one layer for ink B. It took around 35 minutes for this specimen to be printed. The sample for confocal microscopy was printed with the same array but with ink B containing Nile Red, and only three complex layers. For cryo-scanning electron microscopy, an array of 10 x 4 droplets was printed with 3 complex layers in order to facilitate the sample preparation.

Cryo-Scanning Electron Microscopy

Both control and printed samples were prepared for cryo-SEM (FEI/Philips XL30 ESEM-FEG, Philips, UK). Firstly, samples were loaded onto the cryo-SEM sample holder which was lined with colloidal graphite and tissue tick. They were then frozen with slush N_2. The frozen samples were transferred to the preparation stage chamber under the vacuum of 10^{-5} Pa. At this pressure, they were fractured and etched using a Polaron Polarprep control unit (PP7480) at -90°C for 10 minutes. The samples were then coated with platinum by sputtering under Argon atmosphere. The imaging was carried out at -145 °C and 6.3 x 10^{-3} Pa of vacuum and at 5kV voltage.

Confocal Microscopy

A cover slip each was placed on the sample already printed on a glass slide as well as the control sample obtained from the cast film. A Leica DM2500 confocal microscope was used for imaging. Two different objective lenses (10x and 40x) were employed. An oil droplet was placed on the

cover slip (for 40x only) and the focus was adjusted manually. In compliance with the excitation and emission spectra of Nile Red, laser with 532 nm at 100% intensity was used for excitation and emissions in the range of 550 to 700 nm of wavelength were detected for imaging. Focal planes at every 5 μm were imaged across the depth of 250 μm for the printed sample and across the dept of 100 μm for the control sample.

Micro-Computed Tomography

Micro-CT imaging was performed using Bruker SkyScan 1172. The printed sample was cut into 12 mm in length. It was then securely placed vertically on the rotating platform. Various x-ray images of the sample were taken at multiple angles. No filter was used for the x-ray. The experimental parameters have been listed in Table 2 in Supporting Information.

The set of images at different angles was reconstructed by NRecon and CTAn softwares to obtain a 3D image. The control sample, being a soft film was impossible to be imaged using micro-CT in a fashion comparable to the printed sample.

Elemental Analysis

Both control and printed samples were dried under vacuum (12 kPa pressure) at 60°C for 24 hours. They were then ground and dried again for 24 hours under the same conditions. The analysis for CHNS content was performed using FlashSmart Elemental Analyser by Thermo Fischer Scientific. The dried samples were each filled in a small tin capsule. They were then energetically oxidised

(known as dynamic flash combustion) resulting into a gas mixture which was fed into a thermoconductivity detector (TCD) via a chromatographic column. The TCD then generated output signals proportional to the elemental composition of the sample.

Results and Discussion

The viscosity as well as shear stress of ink A and Ink B have been plotted against shear rate in Figure 3. Even at shear rates approaching 10^{-2} s^{-1}, the viscosity values for both inks are significantly lower than 500 Pa.s. This puts the inks within the viscosity limits of valvejet (0.050 – 500 Pa.s). Both inks seem to be shear-thinning, i.e. their viscosities decrease with increasing shear rate. Such effect is relatively more profound in ink B as it contains xanthan, known to be highly shear-thinning.

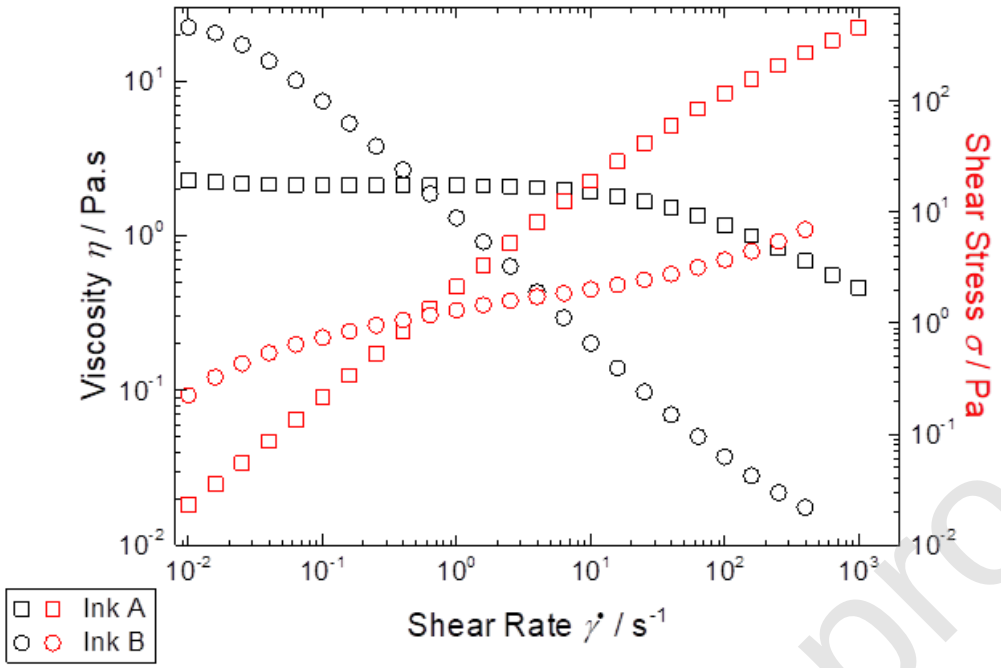

Figure 3. Rheometry data for inks A (2.5% fungal chitosan in 1% acetic acid) and B (8% sodium dodecyl sulphate in 0.1% xanthan gum). Black symbols and red symbols have been used for viscosity and shear stress respectively.

Conventional inkjet printing requires the inks viscosity to be Newtonian and falling within a range between 1 and 40 mPa.s under different shear rates. The shear-thinning nature of inks and their comparatively higher viscosities in the present study hence necessitate the use of pneumatically actuated fluid deposition.

The pH values for inks A and B were found to be 4.6 and 6.8, and the pH for the supernatant within stoichiometric mixture was 4.8. Chitosan can retain positive charge only under pH<6, which is essential for successful formation of SPEC [2].

Following printing, a well-defined shape was obtained with the supernatant solution which was weighed along with the glass slide it was printed on. The supernatant was removed, and the printed shape was weighed again before being imaged as shown in Figure 4:

(a)

(b)

(c)

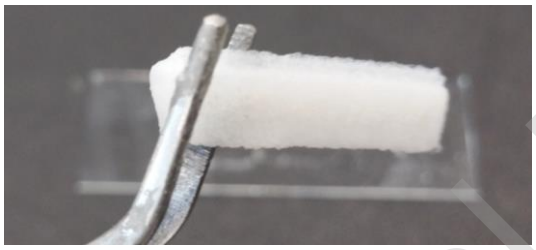

Figure 4. The representative printed specimen as shown by top view (a), side view (b) and held by a pair of tweezers (c). The dimensions are 31.5 mm x 6.9 mm x 1.52 mm. Had there been no supernatant released (which accounted for 49% of the total printed mass), the height of specimen would have been 3.42 mm.

Considering the number of droplets (68 x 14) as well as the droplet spacing (450 μm), the expected dimensions of the footprint of printed specimen are 30.6 mm x 6.3 mm. The actual dimensions of the footprint were found to be 31.5 mm x 6.9 mm, i.e. slightly greater but within 10% of the expected. This discrepancy may be explained by spreading of inks following printing and before the subsequent layer is printed. The thickness of the specimen was 1.52 mm. The weight of the

specimen before and after the removal of supernatant was 0.691 g and 0.352 g respectively, i.e. the solid specimen constituted 51% of the total mass of the mixture. However, the presence of localised regions containing supernatant in the printed specimen cannot be ruled out completely. It is noteworthy that the specimen had sufficient structural integrity to be possible to be picked up by a pair of tweezers.

Images obtained using cryo-SEM for the printed sample have been shown in Figure 5. The presence of cellular structures (diameter ~300 μm) with thick shell walls is somewhat visible in Figure 5 (a) and clearly evident in (b). These observations can be explained by the instantaneous film formation on the droplet (of either inks) surface following its printing over the previously printed layer. The size of so-called cells is within the order of the diameter of the nozzle (150 μm) used for printing the droplets responsible for their formation.

Another striking feature of these images is the fine web-like structure within and around the cells. Such structure has been observed for other systems in the past [31–33], and has been claimed to be a consequence of ice crystal formation during the rapid cooling stage of sample preparation for cryo-SEM. These crystals would have displaced any remaining small amounts of solutes such as polyelectrolyte/surfactant/SPEC in the supernatant to their boundaries. These crystals would then be sublimed during the etching process and leave behind the web-like structures (containing the solutes) as artefacts. The likelihood of such ice crystal formation decreases with lower water content (thus higher solid content) [34]. As a result, the shell walls, presumably formed with precipitated SPEC resist the structural distortion due to ice crystals whereas the supernatant around them with much lower solid content is more prone to this effect.

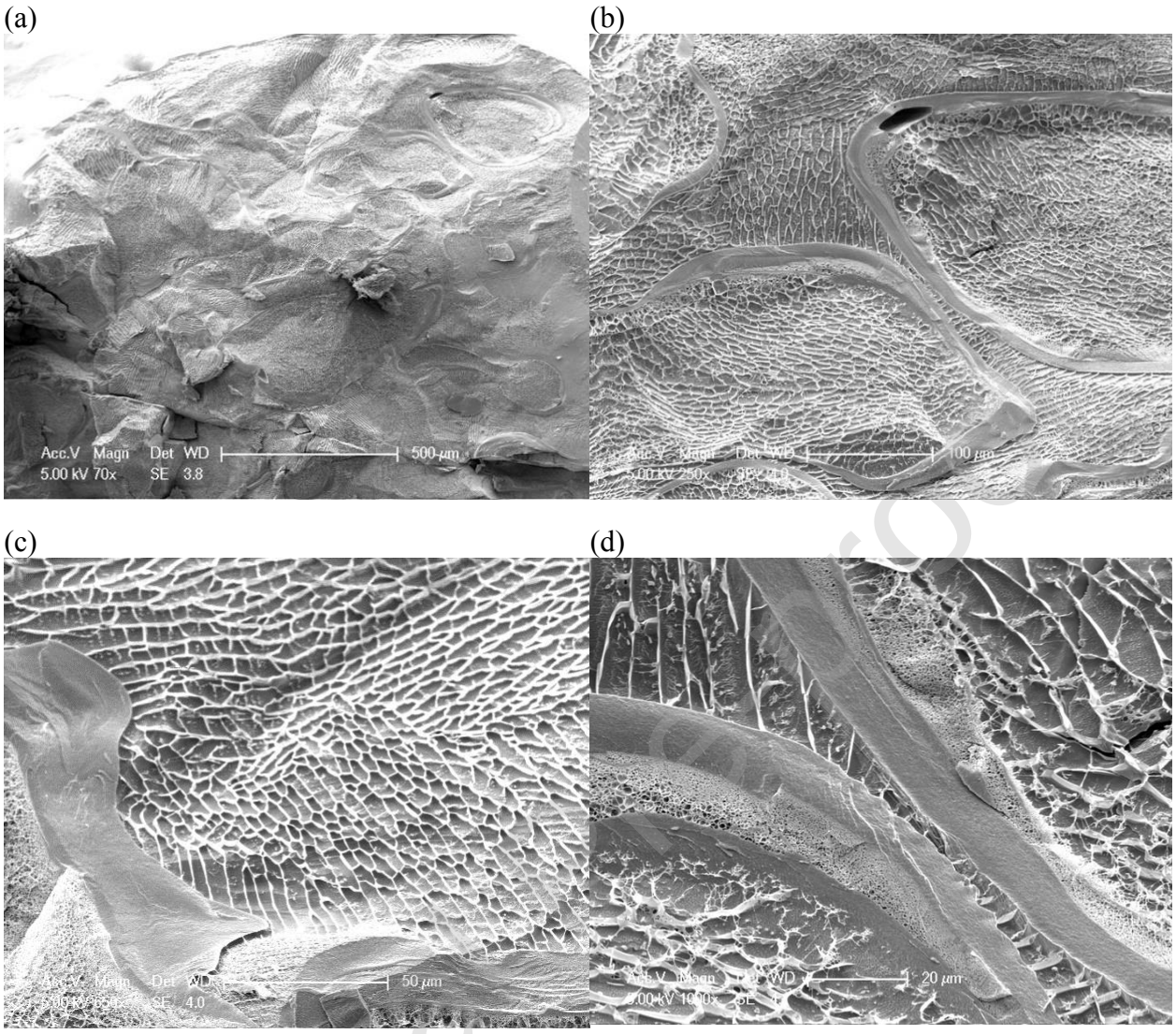

Figure 5. Cryo-SEM images for printed sample at various magnifications. Figure 5 (c) and (d) focus on the shell walls.

However, there is an absence of such cellular structures in the cryo-SEM images of control samples as seen in Figure 6, at both lower and higher magnifications. This leads to the conclusion that in contrast to the printed sample, the solid content in all regions within the control sample is sufficiently high in order to be able to resist the formation of ice crystals. Also, no particular patterns of microstructure are observed in any of the images.

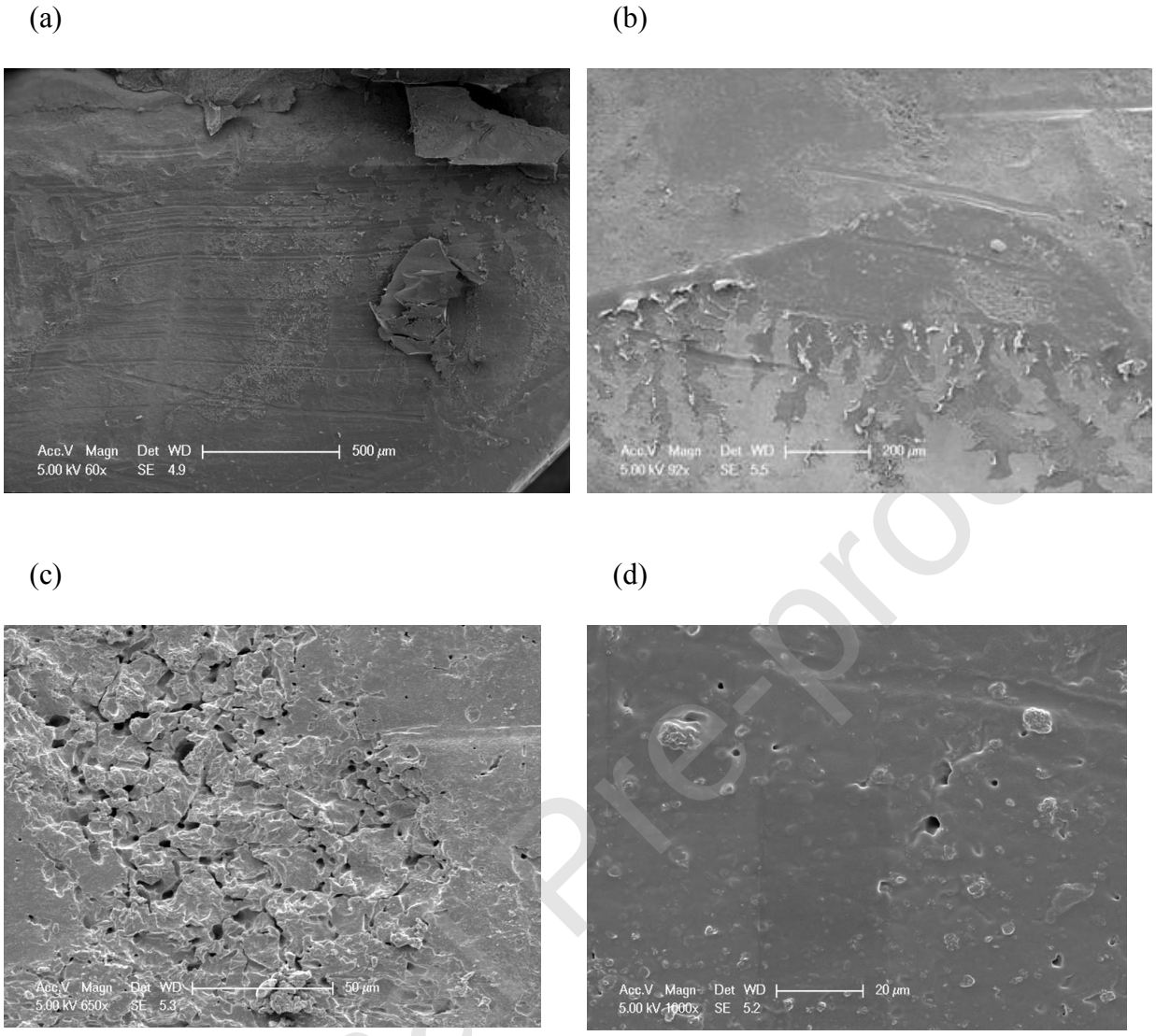

Figure 6. Cryo-SEM images for control sample at various magnifications.

While cryo-SEM images reveal morphological features within the microstructure, they alone cannot be used to determine the composition of these features. To complement cryo-SEM images, confocal microscopy is required as the fluorescent emission of Nile Red can help map the presence of SDS micelles either free in the supernatant or as a part of SPEC across the morphological features.

Figure 7 shows the confocal microscopy images for the printed sample.

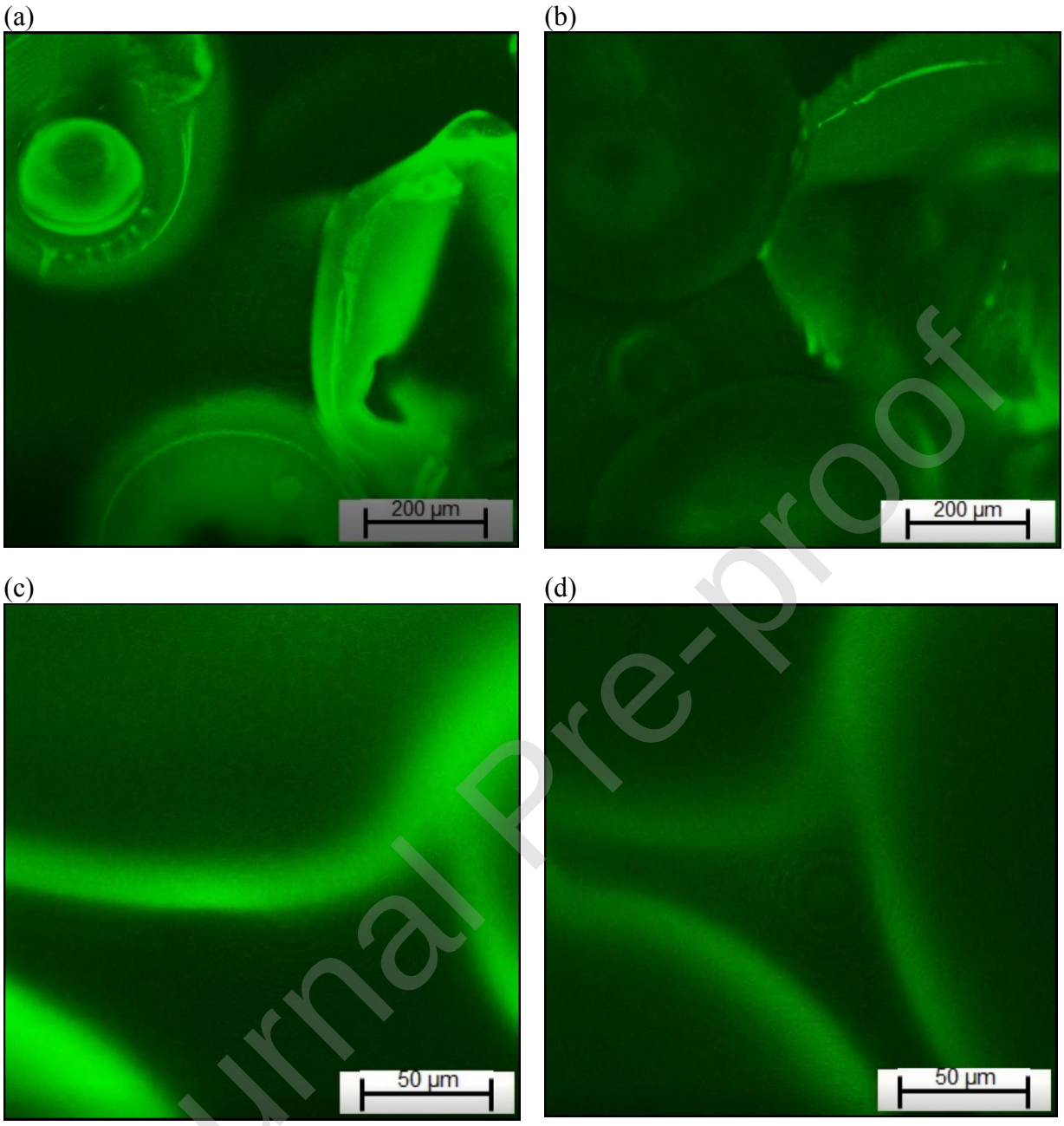

Figure 7. Confocal microscopy images for printed sample at (a) and (b) 10x and (c) and (d) 40x magnifications respectively. Video clips containing these images among those of other layers have been provided in supplementary information.

At 10x magnification, cellular structures with diameters similar to those found in the cryo-SEM images are observed, with bright coloured outer regions and relatively darker cores. The intensity

of light in fluorescence microscopy is proportional to the concentration of the dye given the absorption/emission wavelengths and quantum yield are the same [35]. This further supports the conclusion from cryo-SEM images that the microcapsules consist of micelle-rich shells and relatively micelle-deficient cores. The micelles are expected to have participated in SPEC formation, particularly at the shells owing to them being near the droplet surface during the post-jetting contact with the previously printed layer. Similar observations can be made in images captured at 40x magnification, where the bright shells of microcapsules are seen converging at their junction. Confocal images of SPEC microcapsules comparable to these have already been reported in the past [6,7,36,37], and were also claimed to have SPEC-rich shell and relatively SPEC-deficient core.

As opposed to the printed sample, no discernible microstructural features are observed in the control sample. Although SPEC have been formed in both printed and control samples, the nature of colloidal self-assembly has been very different between them. This echoes the observation from cryo-SEM images.

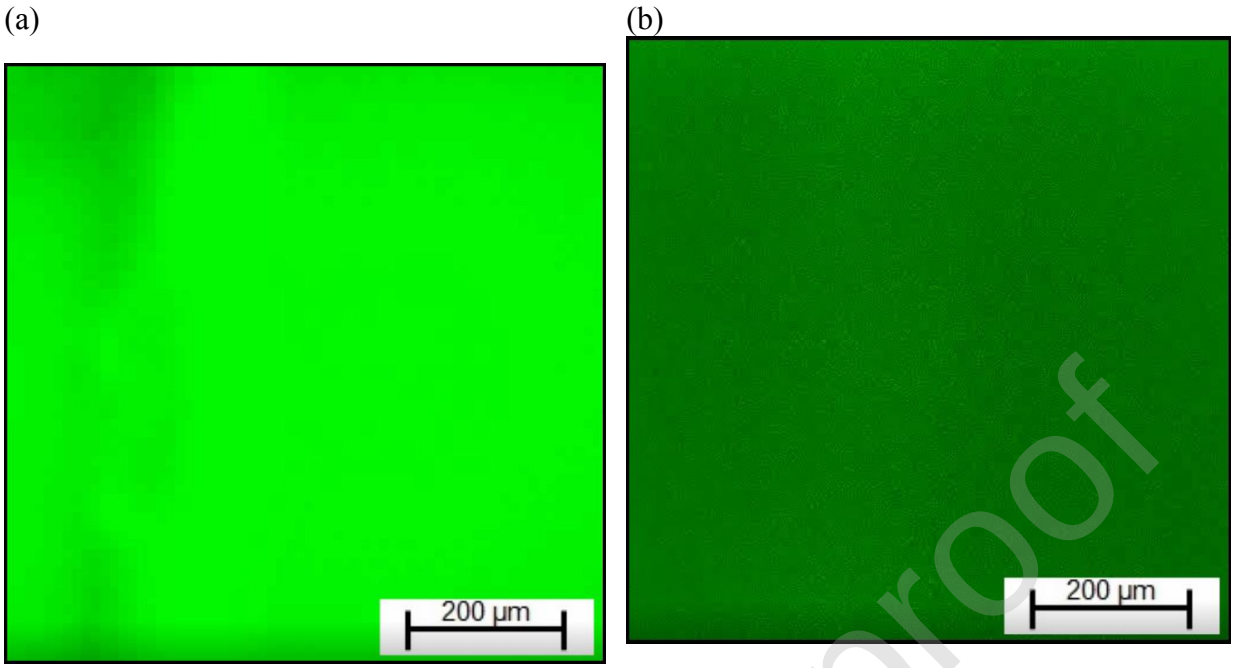

Figure 8. Confocal microscopy images of cast sample at 10x magnification at (a) top and (b) near bottom.

Moreover, the intensity of green colour (which indicates the presence of Nile Red – in SDS micelles) is higher within the top section (i.e. near the interface of two inks) of the sample which decreases gradually across the height, vanishing to nearly zero at the bottom. Decreasing intensity of colour thus strongly suggests a gradual decrease in the dye concentration from above to below (i.e. from the interface of inks A and B to within the bulk of the region on the side of ink A).

As mentioned earlier, the film of SPEC forms almost immediately at the interface of the solutions of oppositely charged polyelectrolyte and surfactant which grows in thickness gradually. It is obvious that with the increase in thickness, permittivity of either polyelectrolyte chains or surfactant micelles through the SPEC film would continue to decrease. Increasingly poor diffusion of either of the components would make the increase in film thickness self-limiting with a concentration gradient of the components across the film. Hence the resultant cast film is likely to

have an excess of surfactant to polyelectrolyte at one surface (the surface close to surfactant solution), and an excess of polyelectrolyte to surfactant at the other. Considering the above, gradual decrease in colour intensity from top to bottom is expected. The video clips depicting the entire sets of confocal microscopic images (from top of the sample to the bottom) for printed sample at both 10x and 40x magnification and for cast sample at 10x magnification can be found in the supplementary information.

Whilst techniques such as cryo-SEM and confocal microscopy are particularly useful at revealing morphological details, their focus on much smaller area begs the question as to whether their observations are representative of the sample in its entirety or are simply manifestations of localised artefacts in an otherwise heterogenous sample. Hence such imaging often needs to be complemented by other imaging/non-imaging characterisation techniques which either take into account the entire sample or its apparently more representative aliquot.

One of such techniques is micro-CT, which works on the principle of difference in absorption of x-ray by materials with different densities. It is possible to image a macroscopic sample with a volume up to at least 10 ml in its entirety using micro-CT. Images obtained using micro-CT for the printed sample are shown in Figure 9.

(a)

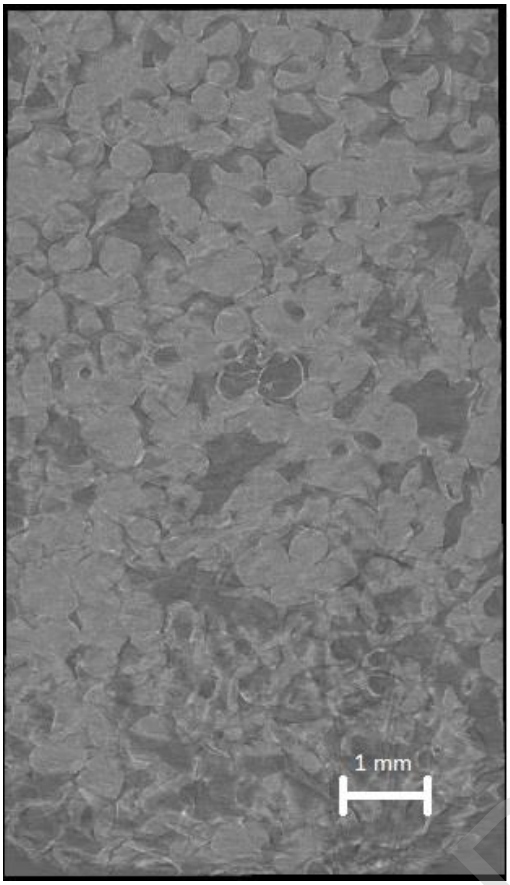

(b)

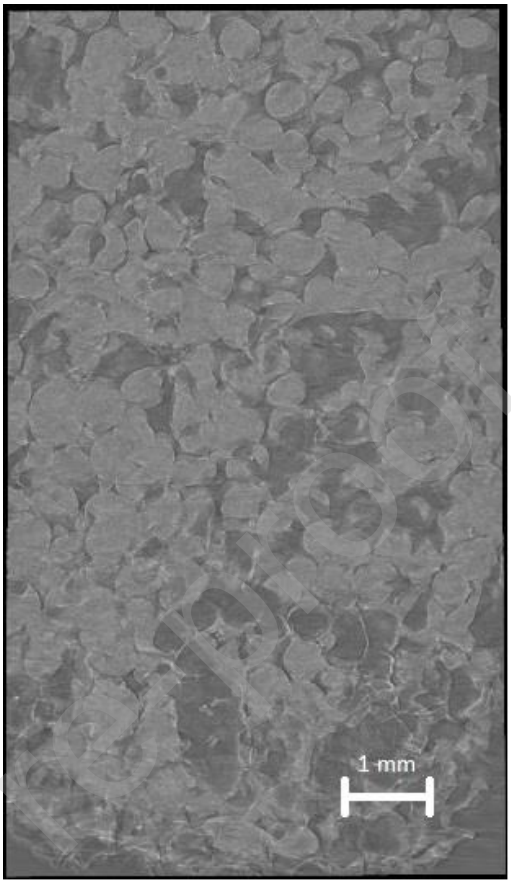

(c)

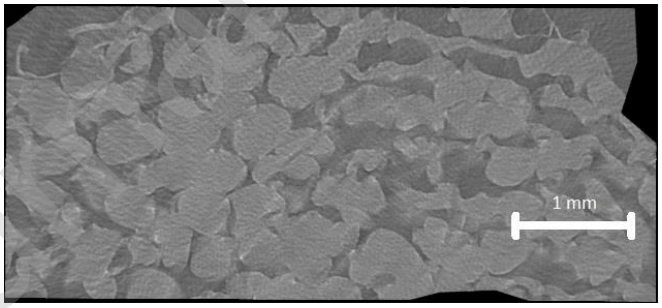

(d)

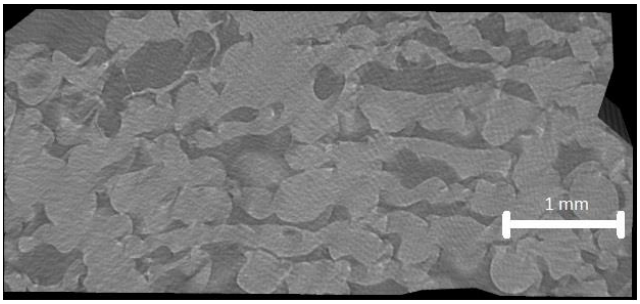

Figure 9. Horizontal (a) and (b) and vertical (c) and (d) cross-sections of printed samples as imaged using micro-CT.

The images in Figure 9 (a) and (b) show two different horizontal cross-sections of the printed sample, representing a printed complex layer each. It is apparent that the complex layers contain cellular-type structures in lighter shades, with interstitial spaces characterised by darker shades. The lighter cellular structures can be attributed to the SPEC microcapsules as observed in the cryo-SEM and confocal microscopy, whereas the darker interstitial spaces manifest the supernatant present. The density difference between the supernatant (presumably close to the density of water) and the SPEC (hydrated precipitates with density higher than that of water) is sufficiently significant for the micro-CT technique to distinguish between themselves. Such structures are consistently spread across the entire layers.

Vertical cross-sections in Figure 9 (c) and (d) represent all printed layers at two different positions. It is evident that the network of microcapsules spans across the height of the printed sample. Moreover, the size of microcapsules (~300 μm) in both horizontal and vertical cross-section is quite consistent with those observed using other techniques.

All repeating units in the chitosan backbone contain one nitrogen atom each, and a vast majority of them constitute deacetylated -NH_2 groups which carry a positive charge each when in an acidic

solution. Conversely, all SDS molecules contain one sulphur atom and one negative charge each. Hence an estimation of N/S elemental ratio in chitosan-SDS SPEC can reveal the status of stoichiometric balance of specimen.

The mean values of N/S ratio for printed and control samples were found to be 1.13 and 0.886 respectively (complete dataset has been shown in the supplementary information). The excess of nitrogen atoms in printed samples can be partly attributed to the still remaining acetylated groups in chitosan which do not carry any positive charge. However, the excess goes much beyond the presence of these 'inactive' nitrogen atoms given that the degree of deacetylation from the manufacturer is ≥ 98.0%. This has also been observed earlier in case of SPEC microcapsules prepared by spraying chitosan solution onto SLES solution where the microcapsules were observed to contain positive charge [4]. In another study, the N/S ratio was observed as high as 2.6 [14]. Since the amount of chitosan and SDS mixed in the present study were balanced stoichiometrically, excess of nitrogen may be explained by poor accessibility of some positively charged repeating units on chitosan backbone owing to its inherent semi-flexible nature resisting sufficient contact with spherical SDS micelles.

The excess of sulphur in the control sample can be interpreted as the SPEC at the interface of chitosan and SDS solutions during the film casting being very SDS-rich. This may be partly due to its proximity to the SDS solution as well the poor diffusion of SDS away from the interface.

Conclusions

The surfactant-polyelectrolyte complex prepared by film casting (control) were compared with those printed using valvejet through various imaging techniques and elemental analysis. It became apparent that the control sample had a continuous matrix with compositional gradient across its thickness. The concentration of surfactant (as micelles) was the highest at the top of the film, vanishing to near zero at the bottom of the film. This gradient was attributed to increasingly poor diffusion of surfactant across the film thickness.

On the other hand, the printed sample had a network of microcapsules spanning across its entire dimensions. These microcapsules had diameters around 300 μm and were a result of alternating deposition of thin layers made of two-dimensional arrays of droplets of inks A and B. This difference in the microstructure of both samples was attributed to more efficient colloidal self-assembly in case of printed samples.

The resultant microstructure of the printed sample has not been observed in SPEC before, according to the best of the authors' knowledge. While distinct SPEC microcapsules have been reported in the past, their network spanning a macroscopic specimen with structural integrity sufficient for it to be lifted by a pair of tweezers significantly widens the scope of applications, e.g. in chewable foods or tablets to deliver active compounds. SPEC in general and microcapsules in particular have potential as delivery vehicles for active ingredients of interest such as drugs, flavours, nutrients and genes. For example, the ability to customise a 3D network of microcapsules in layer-wise fashion enables one to load (i) different active agents in different layers or (ii) different amounts of the same active agent in different layers, in specific order. Gradual decay of such SPEC may result into well-orchestrated periodic release of said active ingredient(s).

Valvejet-based 3D printing of SPEC can be extended to different pairs of surfactant and polyelectrolytes, and indeed even to a single type of surfactant with many different polyelectrolytes or vice versa, to suit the application in question. The sheer versatility offered by 3D printing as a technique to a class of materials as diverse as SPEC renders the combination as a vital area for further investigation.

Funding Sources

This work was supported by the Engineering and Physical Sciences Research Council [grant number EP/N024818/1], funded at the University of Nottingham.

Author Contributions

Saumil Sudhir Vadodaria – Conceptualization, Investigation, Writing – Original Draft.
Yinfeng He – Methodology, Resources, Writing – Review and Editing.

Thomas Mills and **Ricky Wildman** – Supervision, Writing – Review and Editing, Funding Acquisition.

Data Availability

The data in form of images has been used as recorded, hence it can be found from the manuscript itself. For confocal microscopy, the recorded videos from which the images have been taken are provided in the supporting information.

Declaration of interests

The authors declare that they have no known competing financial interests or personal relationships that could have appeared to influence the work reported in this paper.

References

[1] L. Chiappisi, M. Gradzielski, Co-assembly in chitosan-surfactant mixtures: Thermodynamics, structures, interfacial properties and applications, Adv. Colloid Interface Sci. 220 (2015) 92–107. doi:10.1016/j.cis.2015.03.003.

[2] M. Rinaudo, N.R. Kil'deeva, V.G. Babak, Surfactant-polyelectrolyte complexes on the basis of chitin, Russ. J. Gen. Chem. 78 (2008) 2239–2246. doi:10.1134/S1070363208110455.

[3] Y. Lapitsky, T. Zahir, M.S. Shoichet, Modular biodegradable biomaterials from surfactant and polyelectrolyte mixtures, Biomacromolecules. 9 (2008) 166–174. doi:10.1021/bm7009416.

[4] S. Peretz, M. Florea-Spiroiu, D.F. Anghel, C. Munteanu, D. Angelescu, C. Stoian, G. Zgherea, Chitosan-sodium lauryl ether sulfate particles and their use for adsorption of Cu(II) ions, J. Appl. Polym. Sci. 131 (2014) 1–8. doi:10.1002/app.40059.

[5] V.G. Babak, E.A. Merkovich, L.S. Galbraikh, E. V Shtykova, M. Rinaudo, Kinetics of diffusionally induced gelation and ordered nanostructure formation in surfactant-polyelectrolyte complexes formed at water/water emulsion type interfaces, Mendeleev Commun. 10 (2000) 94–95. http://www.sciencedirect.com/science?_ob=ArticleURL&_udi=B8G3W-4S257JN-7&_user=10&_coverDate=12/31/2000&_rdoc=1&_fmt=high&_orig=gateway&_origin=gateway&_sort=d&_docanchor=&view=c&_searchStrId=1677684879&_rerunOrigin=google&_acct=C000050221&_version=1&_url.

[6] Y. Lapitsky, E.W. Kaler, Formation and structural control of surfactant and polyelectrolyte gels, Colloids Surfaces A Physicochem. Eng. Asp. 250 (2004) 179–187. doi:10.1016/j.colsurfa.2006.01.017.

[7] U. Manna, S. Patil, Dual drug delivery microcapsules via layer-by-layer self-assembly, Langmuir. 25 (2009) 10515–10522. doi:10.1021/la901243m.

[8] V.G. Babak, E.A. Merkovich, J. Desbrières, M. Rinaudo, Formation of an ordered nanostructure in surfactant- polyelectrolyte complexes formed by interfacial diffusion, Polym. Bull. 81 (2000) 77–81.

[9] T.D.A. Senra, S.P. Campana-Filho, J. Desbrières, Surfactant-polysaccharide complexes based on quaternized chitosan. Characterization and application to emulsion stability, Eur. Polym. J. 104 (2018) 128–135. doi:10.1016/j.eurpolymj.2018.05.002.

[10] L. Petrović, J. Milinković, J. Fraj, S. Bučko, J. Katona, L. Spasojević, Study of interaction between chitosan and sodium lauryl ether sulfate, Colloid Polym. Sci. 295 (2017) 2279–2285. doi:10.1007/s00396-017-4205-7.

[11] L. Chiappisi, S. Prevost, I. Grillo, M. Gradzielski, From Crab Shells to Smart Systems: Chitosan - Alkylethoxy Carboxylates Complexes., Langmuir. 30 (2014). doi:10.1021/la502569p.

[12] V.G. Babak, J. Desbrieres, Dynamic surface tension and dilational viscoelasticity of adsorption layers of alkylated chitosans and surfactant-chitosan complexes, Colloid Polym. Sci. 284 (2006) 745–754. doi:10.1007/s00396-005-1427-x.

[13] U. Manna, S. Patil, Encapsulation of uncharged water-insoluble organic substance in polymeric membrane capsules via layer-by-layer approach, J. Phys. Chem. B. 112 (2008) 13258–13262. doi:10.1021/jp806140s.

[14] H. He, X. Cao, H. Dong, T. Ma, G.F. Payne, Reversible Programing of Soft Matter with Reconfigurable Mechanical Properties, Adv. Funct. Mater. 27 (2017). doi:10.1002/adfm.201605665.

[15] M. Wu, N. An, Y. Li, J. Sun, Layer-by-Layer Assembly of Fluorine-Free Polyelectrolyte-Surfactant Complexes for the Fabrication of Self-Healing Superhydrophobic Films, Langmuir. 32 (2016) 12361–12369. doi:10.1021/acs.langmuir.6b02607.

[16] X. Huang, N.S. Zacharia, Surfactant co-assembly and ion exchange to modulate polyelectrolyte multilayer wettability, Soft Matter. 9 (2013) 7735–7742. doi:10.1039/c3sm50782c.

[17] C.M. Andres, N.A. Kotov, Inkjet Deposition of Layer-by-Layer Assembled Films, 38 (2010) 14496–14502.

[18] I.C. Gîfu, M.E. Maxim, A. Iovescu, E.L. Simion, L. Aricov, M. Anastasescu, C. Munteanu, D.F. Anghel, Surface hydrophobization by electrostatic deposition of hydrophobically modified poly(acrylates) and their complexes with surfactants, Appl. Surf. Sci. 371 (2016) 519–529. doi:10.1016/j.apsusc.2016.03.036.

[19] C. Gustavsson, J. Li, K.J. Edler, L. Piculell, Water-responsive internally structured polymer-surfactant films on solid surfaces, Langmuir. 30 (2014) 12525–12531. doi:10.1021/la503210g.

[20] H. Yang, Y. He, C. Tuck, R. Wildman, I. Ashcroft, P. Dickens, R. Hague, High viscosity jetting system for 3D reactive inkjet printing, in: 24th Annu. Int. Solid Free. Fabr. Symp. - an Addit. Manuf. Conf., University of Texas, Austin, Texas, 2013: pp. 505–513.

[21] B. Bonhoeffer, A. Kwade, M. Juhnke, Impact of Formulation Properties and Process Parameters on the Dispensing and Depositioning of Drug Nanosuspensions Using Micro-

Valve Technology, J. Pharm. Sci. 106 (2017) 1102–1110. doi:10.1016/j.xphs.2016.12.019.

[22] F. Liravi, E. Toyserkani, A hybrid additive manufacturing method for the fabrication of silicone bio-structures: 3D printing optimization and surface characterization, Mater. Des. 138 (2018) 46–61. doi:10.1016/j.matdes.2017.10.051.

[23] J. Ledesma-Fernandez, C. Tuck, R. Hague, High Viscosity Jetting of Conductive and Dielectric Pastes for Printed Electronics, in: Proc. Solid Free. Fabr. Symp., University of Texas, Houston, Texas, 2015: pp. 40–55.

[24] R. Daly, T.S. Harrington, G.D. Martin, I.M. Hutchings, Inkjet printing for pharmaceutics - A review of research and manufacturing, Int. J. Pharm. 494 (2015) 554–567. doi:10.1016/j.ijpharm.2015.03.017.

[25] M. Alomari, F.H. Mohamed, A.W. Basit, S. Gaisford, Personalised dosing: Printing a dose of one's own medicine, Int. J. Pharm. 494 (2015) 568–577. doi:10.1016/j.ijpharm.2014.12.006.

[26] B. Bonhoeffer, A. Kwade, M. Juhnke, Alternative Manufacturing Concepts for Solid Oral Dosage Forms From Drug Nanosuspensions Using Fluid Dispensing and Forced Drying Technology, J. Pharm. Sci. 107 (2018) 909–921. doi:10.1016/j.xphs.2017.11.007.

[27] L.B. Petrović, J.R. Milinković, J.L. Fraj, S.D. Bučko, J.M. Katona, An investigation of chitosan and sodium dodecyl sulfate interactions in acetic media, J. Serbian Chem. Soc. 81 (2016) 575–587. doi:10.2298/JSC151119024P.

[28] G.S. Dhillon, S. Kaur, S.K. Brar, M. Verma, Green synthesis approach: Extraction of chitosan from fungus mycelia, Crit. Rev. Biotechnol. 33 (2013) 379–403. doi:10.3109/07388551.2012.717217.

[29] J.E. Desbrieres, C. Bousquet, V. Babak, J. Desbrières, J. Desbrieres, Surfactant-chitosan

interactions and application to emulsion stabilization, Cellul. Chem. Technol. 44 (2010) 395–406. http://apps.webofknowledge.com/full_record.do?product=UA&search_mode=Refine&qid=3&SID=Z2URoWzSWyffrIlZ7ig&page=1&doc=1%5Cnhttp://apps.webofknowledge.com/full_record.do?product=UA&search_mode=CitingArticles&qid=3&SID=U2M5K42OA2Am4gg9El1&page=1&doc=7.

[30] I.N. Kurniasih, H. Liang, P.C. Mohr, G. Khot, J.P. Rabe, A. Mohr, Nile red dye in aqueous surfactant and micellar solution, Langmuir. 31 (2015) 2639–2648. doi:10.1021/la504378m.

[31] L. Ong, R.R. Dagastine, S.E. Kentish, S.L. Gras, Microstructure of milk gel and cheese curd observed using cryo scanning electron microscopy and confocal microscopy, LWT - Food Sci. Technol. 44 (2011) 1291–1302. doi:10.1016/j.lwt.2010.12.026.

[32] C. Efthymiou, M.A.K. Williams, K.M. McGrath, Revealing the structure of high-water content biopolymer networks: Diminishing freezing artefacts in cryo-SEM images, Food Hydrocoll. 73 (2017) 203–212. doi:10.1016/j.foodhyd.2017.06.040.

[33] P. Sriamornsak, N. Thirawong, K. Cheewatanakornkool, K. Burapapadh, W. Sae-Ngow, Cryo-scanning electron microscopy (cryo-SEM) as a tool for studying the ultrastructure during bead formation by ionotropic gelation of calcium pectinate, Int. J. Pharm. 352 (2008) 115–122. doi:10.1016/j.ijpharm.2007.10.038.

[34] R. Aston, K. Sewell, T. Klein, G. Lawrie, L. Grøndahl, Evaluation of the impact of freezing preparation techniques on the characterisation of alginate hydrogels by cryo-SEM, Eur. Polym. J. 82 (2016) 1–15. doi:10.1016/j.eurpolymj.2016.06.025.

[35] J.B. Pawley, Handbook of biological confocal microscopy: Third edition, 2006. doi:10.1007/978-0-387-45524-2.

[36] T. Obfs, B.Z. Dai, A. Voigt, S. Leporatti, E. Donath, Layer-by-Layer Self-Assembly of Polyelectrolyte, Adv. Mater. (2001) 1339–1342.

[37] E. Donath, G.B. Sukhorukov, F. Caruso, S.A. Davis, H. Möhwald, Novel Hollow Polymer Shells by Colloid-Templated Assembly of Polyelectrolytes, Angew. Chemie Int. Ed. 37 (1998) 2201–2205. doi:10.1002/(SICI)1521-3773(19980904)37:16<2201::AID-ANIE2201>3.0.CO;2-E.